Electrostatically Induced Phononic Crystal

D. Hatanaka,[1,*] A. Bachtold,[2] and H. Yamaguchi[1]

[1] *NTT Basic Research Laboratories, NTT Corporation, Atsugi-shi, Kanagawa 243-0198, Japan*

[2] *ICFO-Institut de Ciencies Fotoniques, The Barcelona Institute of Science and Technology, Castelldefels (Barcelona) 08860, Spain*

(Received 27 July 2018; revised manuscript received 14 December 2018; published 8 February 2019)

The possibility of realizing an electrostatically induced phononic crystal is numerically investigated in an acoustic waveguide based on a graphene sheet that is suspended over periodically arrayed electrodes. The application of dc voltage to these electrodes exerts an electrostatic force on the graphene and this results in the periodic formation of stress in the waveguide structure in a noninvasive way, unlike the cases with mass loading and air holes. This noninvasive scheme enables a band gap, namely a phononic crystal, to be created in the waveguide that can be used to dynamically tune the acoustic transparency in the medium. Our approach will allow the dispersion relation to be locally modified, thus modulating the response of traveling acoustic phonon waves. This alternate phonon architecture is promising in terms of realizing advanced control of phonon dynamics such as waveform engineering.

DOI: 10.1103/PhysRevApplied.11.024024

I. INTRODUCTION

A phononic crystal (PnC) is a promising platform for tailoring the dispersion relation of acoustic phonon waves and engineering the transmission properties [1–3]. Hence, the advent of this artificial phonon architecture has attracted considerable interest in phononics [4–9]. The goal in the field is to develop highly functional phononic devices such as signal processors [10] and ultrahigh Q mechanical oscillators [11], and to open up possible applications in topological physics [12–14], thermal management [15–17], and electro- and optomechanics [18–20].

To further increase the functionality of these devices, intensive effort has been devoted to developing dynamic PnCs that allow the temporal control of acoustic waves with an external stimulus. Most of these PnCs have been based on macroscale solid-fluid [21,22] or sonic crystals [23]. In contrast, a chip-based PnC platform has recently been demonstrated that consists of a membrane resonator array with a GaAs/(Al, Ga)As heterostructure [24,25] and a SiN_x film [26]. The ability to dynamically control acoustic waves by using the mechanical nonlinearity and electrostatic effect in the devices has made it possible to realize functional acoustic devices [27,28]. However, these devices suffer from low breakdown in the GaAs-piezoelectric transduction and the narrow operation bandwidth. Additionally, the formation of the band gap still relies on their passive geometric structure, such as air holes and electrode array, which also determines the fundamental limitation of the dynamic control.

One of the keys to overcoming these difficulties is to use an electromechanical resonator based on graphene [29–33] and other two-dimensional (2D) materials [34]. This is because these layered materials host a low mass and a large Young's modulus ($m_{\mathrm{eff}} \sim 10^{-17}$ kg and $E = 1$ TPa in graphene, respectively [30,35]), that enhance the mode-coupling nonlinearity of the resonator ($\propto E/m_{\mathrm{eff}}$) [36]. Additionally, they have extremely low rigidity that enables them to be stretched significantly by employing modest electrostatic force. This deformation induces stress without any invasive physical contact and realizes large mechanical tunability. As a result, the electrically active phonon systems using graphene and other 2D materials have demonstrated a range of dynamic control over acoustic resonant vibrations including coherent manipulation between different modes [32,33] and the possibility to tune the operating frequency by a large amount [29–33].

We propose an electrostatically induced PnC based on graphene-electromechanical systems, and we investigate the properties using the finite element method (FEM). The application of a dc voltage to a gate electrode array underneath a suspended graphene waveguide (WG) exerts electrostatic force on the graphene, which induces bending toward the electrodes [29–34]. This electrostatic stretching forms a periodic elastic potential in the WG and modulates the dispersion relation of traveling acoustic waves, enabling band gaps to be noninvasively created. Consequently, this noninvasive approach can realize a dynamic transition in the acoustic conduction property

*daiki.hatanaka.hz@hco.ntt.co.jp

from transparency to opacity, that is, from WG to PnC. This will also enable the temporal control of group velocity and the trapping of the acoustic waves in an arbitrary position. Thus, the graphene-based phonon architecture will open up possible applications in the fields of signal processing and electromechanics.

II. DEVICE DESIGN

The device consists of a graphene multilayer with a thickness $t = 25 \times t_g = 8.5$ nm (t_g is the thickness of a graphene monolayer, 0.34 nm) and density $\rho = \eta \times 2235$ kg/m^3 (η is a correction factor for contamination on a graphene surface, $\eta = 4.5$ is used in this study [30]). The graphene sheet is suspended over a rectangular trench of length L and width $w = 3.2$ μm ($L \gg w$) fabricated from an insulating material such as SiO_2 as shown in Fig. 1(a). A gate electrode with the dimensions (w_{gx}, w_{gy}) = (1.60 μm, 2.88 μm) is periodically arrayed with a pitch of $a = 3.2$ μm at the bottom of the trench and the electrodes are spatially separated in vacuum from the suspended graphene by a distance of approximately $d = 85$–180 nm. The geometric parameters used in this study are typical values taken from previous experimental studies on individual mechanical resonators [30,31].

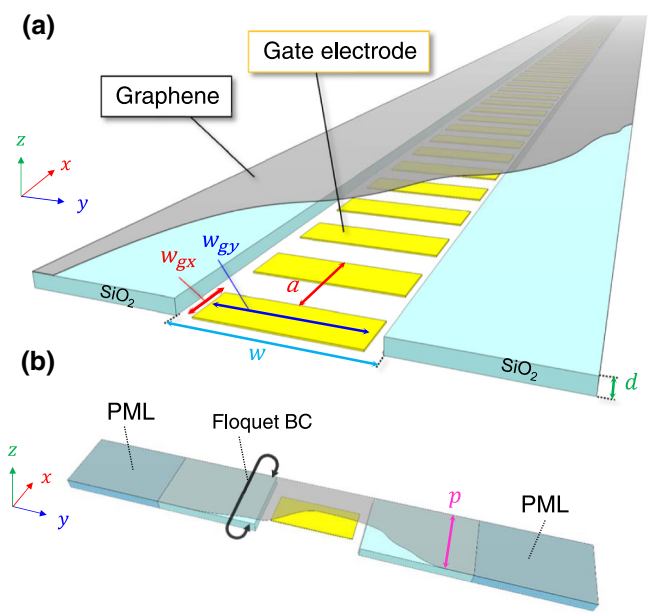

FIG. 1. (a) A schematic of a graphene-based acoustic WG where the graphene film is suspended over a trench with a gate electrode array at its bottom. Electrodes with the dimensions $w_{gx} \times w_{gy}$ are periodically arrayed with a distance of a between them. Graphene with a thickness t is suspended by a trench with a width w and is spatially separated from the gate electrodes by a distance d. (b) A unit structure having a length p that is a periodic distance between voltage-biased electrodes. The Floquet boundary condition (BC) is used to calculate the dispersion relation. Perfect matched layers (PMLs) are introduced to avoid undesired reflection.

An electrostatic pressure P_{es} can be induced by applying a dc electric voltage to the gate electrodes and it is calculated by

$$P_{es} = \frac{1}{2}\frac{dC_u}{dz}V_g^2 = \frac{1}{2}\frac{\varepsilon_0}{(d - z_s)^2}V_g^2, \tag{1}$$

where C_u, ε_0, and z_s are the capacitance per unit area formed between the graphene and the gate electrode, the vacuum permittivity, and the static displacement of the graphene induced by the electrostatic force, respectively. The electromechanical properties and dispersion relation are simulated in the unit structure of the WG with COMSOL MULTIPHYSICS 5.3 as shown in Fig. 1(b). Note that in the simulation, the graphene unit structure is given a fixed boundary at the bottom of the SiO_2 mesa substrate and Floquet periodic conditions at $(x, y) = (\pm p/2, y)$, respectively. Here, p is the separation between the electrodes to which we apply the gate voltage. The graphene structure has sixfold rotation symmetry and the graphene multilayer is described as an isotropic continuum elastic medium with Young's modulus $E = 1$ TPa [35] and Poisson ratio $\nu = 0.16$ [37]. To avoid undesired reflection, a perfect matched layer (PML) is introduced into the outer domain of both mesa structures.

III. SIMULATION RESULTS

A. Electromechanical property

To understand the static electromechanical property of the device, we consider a unit structure with two electrodes of unit length $p = 2a$ and investigate the mechanical deformation of the graphene when we apply a gate voltage V_g to one of the two electrodes as shown in Fig. 2(a). The application of the gate voltage concentrates the electric field between the graphene and the electrode, which exerts an electrostatic force on the graphene, thus bending it toward the electrode as shown by the solid gray line in Fig. 2(b). The static deformation z_s increases when decreasing the gate separation d as shown in Fig. 2(c). The largest displacement z_s^{max} of the graphene along the trench axis is between 19.2 and 7.2 nm for a distance d between 85 and 180 nm. Such large deformations cannot be achieved with conventional mechanical devices. This deformation induces large stress in the suspended graphene WG, which increases to 395 MPa at the edges when $d = 85$ nm and $V_g = 5$ V, as shown in Fig. 2(e). These deformation and stress can also be adjusted by changing the gate voltage V_g as shown in Figs. 2(d) and 2(f). The results reveal that the electrostatic graphene WG devices enable the generation of periodic stress and elastic potential variations in a noninvasive way, in contrast to previous works where such an elastic inhomogeneity was induced by loading mass and making air holes [3].

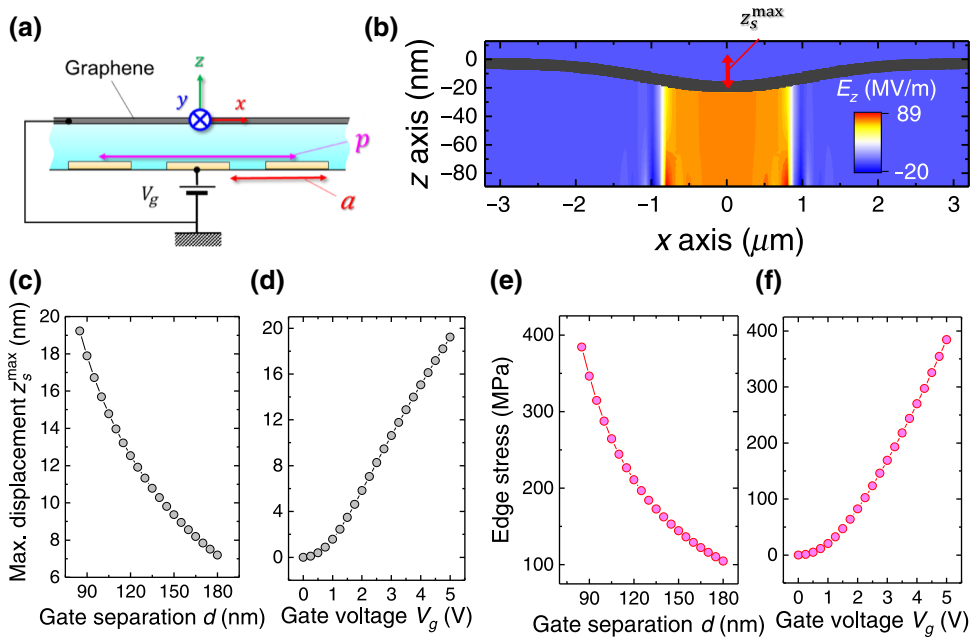

FIG. 2. (a) A schematic showing the cross section of the unit structure of the graphene WG used for FEM calculations. The unit length along the x axis is $p = 2a = 6.4$ μm. Here, the dc gate voltage is applied between one electrode and the graphene. (b) Electric field distribution and static displacement of the graphene sheet along the x axis. The electric field in the z direction E_z is represented on the x-z plane at $y = 0$ when applying $V_g = 5$ V. The field E_z is strongly confined in a vacuum gap with $d = 85$ nm between the electrode and graphene. This exerts electrostatic force on the graphene and bends it toward the electrode (gray line). (c),(d) The gate-graphene separation d and the gate voltage V_g dependence of the maximum static displacement z_s^{max} [see (b)], respectively. (e),(f) The gate-graphene separation d and the gate voltage V_g dependence of the stress at clamping edges $(x, y) = (0, \pm w/2)$, respectively. They are electrostatically induced by $V_g = 5$ V [(c) and (e)] and create the separation $d = 85$ nm [(d),(f)].

B. Formation of band gap

The emergence of the phononic band gap results from the Bragg reflection of acoustic waves traveling in the periodic elastic potential. Here, we investigate the electrostatic effect on the band dispersion in the WG. Figure 3 shows the dispersion relation in the device at various gate voltages. It exhibits parabolic dispersion curves at the gate voltage $V_g = 0$ V as shown in the first panel from the left in Fig. 3, which is a trivial property of a normal WG structure. However, an increase in the gate voltage to $V_g = 2$ and 4 V results in a sizeable effect of the electrostatically induced periodic stress on the dispersion curve with the formation of band gaps as shown in the second and third panels in Fig. 3. By further increasing the gate voltage to $V_g = 6$ and 8 V, the spectral width of the band gaps is broadened and the dispersion curves become flattened as shown in the fourth and fifth panels in Fig. 3, respectively.

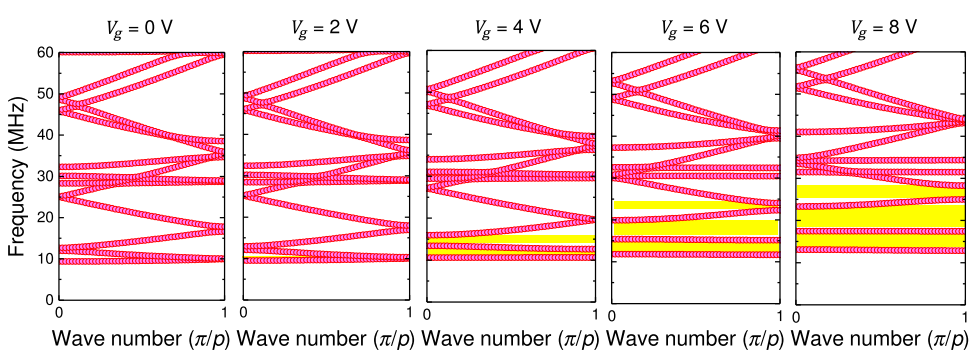

FIG. 3. The dispersion relation of the graphene-based WG with $d = 130$ nm at various gate voltages V_gs. The dispersion is simulated by applying the Floquet periodic condition to the unit structure shown in Fig. 2(a). An increase in V_g creates the band gaps (yellow) and the reduction in the dispersion slopes (pink circles).

Our approach can be used to dynamically manipulate the band structure and thus the acoustic wave during propagation.

Perhaps the most important advantage of this scheme is to modify the periodic pitch of the elastic potential by simply changing the configuration of the applied gate voltage. Here, we modify the periodic pitch p between a, $2a$, and $3a$ [Figs. 4(a)–4(c)]. This engineering of the gate-voltage configuration alters the periodic elastic potential and thus enables the dispersion relation to be reconfigured.

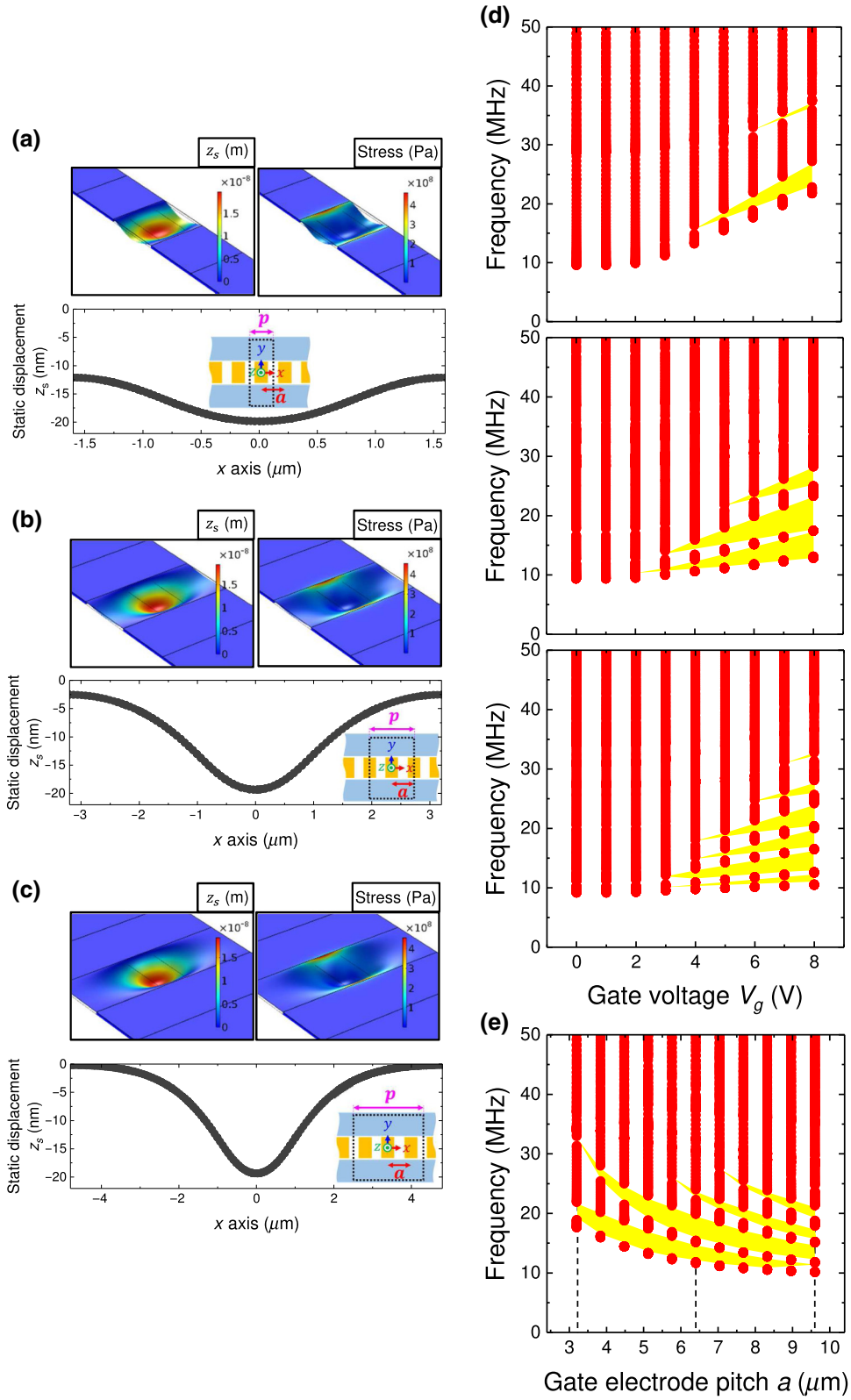

FIG. 4. (a)–(c) The simulated profile of the static displacement z_s (left panel) and stress (right panel) in the unit structure of the graphene WG with $d = 130$ nm and $p = a, 2a$, and $3a$ when applying $V_g = 8$ V. The static displacement z_s in the x-z plane at $y = 0$ as shown in the bottom panel. The inset in the bottom panel is a schematic of the top view and the x-y-z coordinates. The black dotted frame denotes the unit structure with length p. (d) The eigenfrequencies as a function of the gate voltage V_g with $p = a, 2a$, and $3a$ as shown in the top, middle, and bottom panels, respectively. The band gaps are highlighted in yellow. (e) The periodic pitch a dependence of the eigenfrequencies in the device at $V_g = 6$ V. The band gap is highlighted in yellow. The black dashed lines denote $a =$ 3.2, 6.4, and 9.6 μm, where the same configurations are realized as in (a)–(c), respectively.

With $p = a$, the gate electrode separation is short and this causes quasiuniform deformation of the graphene sheet along the x axis so that the entire WG is stretched toward the electrodes. Thus the induced stress is not strongly localized, but is distributed throughout the entire device as shown in Fig. 4(a). Therefore, few band gaps emerge. On the other hand, the cut-off frequency greatly increases when increasing the gate voltage due to the uniform stress as shown in the top panel of Fig. 4(d). By changing the periodic pitch to $p = 2a$ and $3a$, the gate-induced deformation and stress are localized as shown in Figs. 4(b) and 4(c), respectively. As a result, multiple band gaps occur and the cut-off frequencies are less dependent on the gate voltage, as shown in the middle and bottom panels of Fig. 4(d), respectively.

Changing the gate electrode pitch a also modifies the band gaps as shown in Fig. 4(e), where we use $p = a$ and $V_g = 6$ V. This clearly indicates that the spectral position of the band gaps varies and the number of sizeable band gaps increases when increasing pitch a. In particular, when $a = 3.2$, 6.4, and 9.6 μm (dashed lines), the same gate configurations as in Figs. 4(a)–4(c) are realized, respectively. In this way, the electrostatic force induced by the gate electrode array allows the band dispersion in the WG to be designed with the gate voltage configuration.

C. Spectral response

In order to ensure the validity of the band-gap effect, the spectral response of the graphene WG is investigated under the excitation of various V_g. Here, the simulated system is designed to have a length $L = Np = 2Na$, where $N = 32$ and $a = 3.2$ μm as shown in Fig. 5(a). Mechanical vibration is locally excited by applying ac and dc driving voltages, $V_d^{\mathrm{ac}} \cos(2\pi ft)$, where f is frequency and V_d^{dc}, respectively, to the leftmost electrode. Using Eq. (1), harmonic driving pressure P_d exerted on the suspended graphene is given as

$$P_d = \frac{\varepsilon_0}{(d - z_s)^2} V_d^{\mathrm{ac}} V_d^{\mathrm{dc}} \cos(2\pi ft), \tag{2}$$

thus, both ac and dc voltages are required for vibration activation. The excited vibrations are flexural modes due to the extremely small thickness-to-width aspect ratio of the device ($t/w \ll 1$). To reduce computational cost, only part of a suspended graphene WG is prepared in the model where a fixed constraint is the outer edges (see the dotted lines in Fig. 5(a)), and the electrostatic forces P_{es} and P_d in $z_s = 0$ are directly applied to the graphene sheet along the z axis. It is confirmed that the approximation does not produce a critical difference from the previous approaches shown in Figs. 2–4, and it is described in detail in the Supplemental Material [39].

The transmission spectrum through the device is quantified by driving the left side and probing the displacement

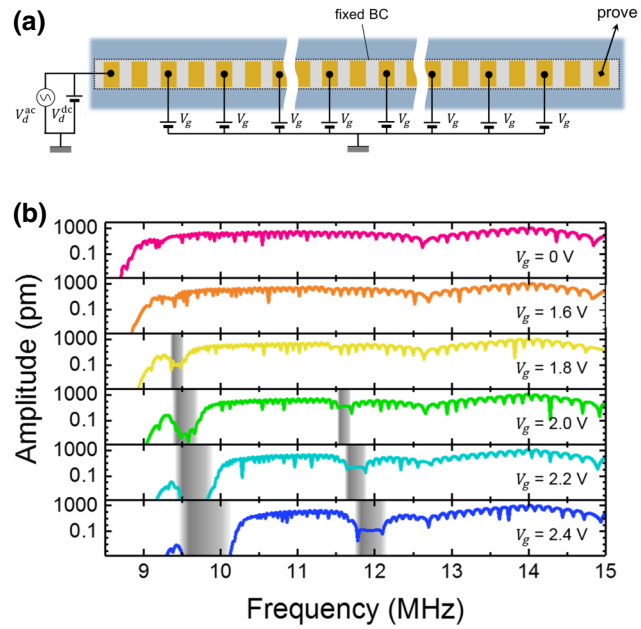

FIG. 5. (a) A schematic showing the top view of the graphene WG. The suspended membrane part is used for calculation where a fixed BC is applied to the edges of the graphene, denoted as the dotted lines. Harmonic vibrations are locally driven from the left side of the WG through the gate electrode with V_d^{ac} and V_d^{dc}, and the resulting vibration is calculated at the graphene above the center of the rightmost electrode. To investigate the electrostatic effect on the transmission property, the gate voltage V_g is uniformly applied to every two gate electrodes, $p = 2a$. An internal loss factor $1/Q \sim 0.01$ is used in the simulations as typically measured in graphene resonators at room temperature [29,33,38]. (b) The frequency response of the graphene WG at the right edge when exciting the left one with $V_d^{\mathrm{ac}} = 0.4$ V and $V_d^{\mathrm{dc}} = 4$ V for different V_g values. The vibration amplitudes are suppressed in some frequency ranges (highlighted in gray) due to the band gap created by applying V_g.

amplitude on the right side [Fig. 5(a)]. Mechanical vibrations up to nanometer-scale displacements are confirmed in continuous bands beyond 8.7 MHz, as shown in the top two panels of Fig. 5(b), and can be detected by using conventional optical interferometer techniques [33,40]. By applying $V_g \geq 1.8$ V, a band gap appears around 9.4 MHz as shown in the third panel from the top. Further increases in V_g to 2.0, 2.2, and 2.4 V enable the band gap to shift to higher frequencies and to feature a transmission that is further suppressed, as shown in the bottom three panels. Moreover, a second band gap is created in the 11.6–12.1 MHz range due to Bragg reflection caused by a second Brillouin zone edge. Thus, the results indicate that the transmission property of the graphene WG can be dynamically adjusted by electrostatic activation.

For experimental realization of the PnC, it would be reasonable to fabricate a WG with $N > 30$. This nearly corresponds to L between 0.1 and 0.3 mm in our model. Such a submillimeter-scale graphene can be obtained by

chemical vapor deposition. The large graphene sample can be suspended by the usual dry-transfer method [41] and the recently developed vacuum stack process [42]. Although the stress that is built in during fabrication might be nonuniform along the WG, this can be compensated for by applying the appropriate V_g to each gate electrode. Thus, we expect that graphene-based PnCs can be realized with existing fabrication techniques.

IV. PROSPECT

This PnC layout offers several advantageous features when compared to conventional PnC devices. First, the PnC band structure is created by the electrostatic force induced by the spatially isolated electrodes. Therefore, this noninvasive approach enables on-demand tuning of the acoustic transparency of the device. Second, the gate voltage configuration determines the band structure. This not only modulates the spectral positions of the band gaps, it can also create a defect cavity at any desired location via local voltage modification. For instance, this can allow the strain distribution at the clamping points to be tailored in the cavity by optimizing the gate voltages, which might be used to realize a Q tunable mechanical resonator [11]. Finally, the electrostatic force can also modify the mechanical nonlinearity of the device, which tunes and enhances the nonlinear parametric effect [36]. The ability to adjust both the nonlinearity and the dispersion of the device can be useful for investigating nonlinear phenomena such as phononic solitons. This is possible because the soliton is generated as a result of the balance between the effects of nonlinear phase modulation and group velocity dispersion on a traveling wave [43]. The control of both effects holds promise for the demonstration of the dynamic manipulation of the temporal and spectral waveforms of an acoustic wave.

V. CONCLUSION

In conclusion, we propose a PnC structure where the periodic stress profile can be noninvasively induced in a suspended graphene WG by applying a dc voltage to a gate electrode array. As a result, the dispersion relation is modulated and band gaps are generated. Moreover, the spectral position and width of the band gaps can be controlled by varying the periodic arrangement of the gate voltage application. The ability to dynamically engineer the band structures opens up the possibility of developing various acoustic devices for signal processing applications. This approach can be also used to study different nonlinear phononic phenomena and to construct highly functional electromechanical circuits.

ACKNOWLEDGMENTS

This work was supported by a MEXT Grant-in-Aid for Scientific Research on Innovative Areas "Science of hybrid quantum systems" (Grants No. JP15H05869 and No. JP15K21727), the Foundation Cellex, the CERCA Programme, AGAUR, Severo Ochoa (Grant No. SEV-2015-0522), Grant No. FIS2015-69831-P of MINECO, and the Fondo Europeo de Desarrollo Regional (FEDER).

[1] V. Narayanamurti, H. L. Störmer, M. A. Chin, A. C. Gossard, and W. Wiegmann, Selective Transmission of High-frequency Phonons by a Superlattice: The "Dielectric" Phonon Filter, Phys. Rev. Lett. **43**, 2012 (1979).

[2] R. Martínez-Sala, J. Sancho, J. V. Sánchez, V. Gómez, J. Llinares, and F. Meseguer, Sound attenuation by sculpture, Nature **378**, 241 (1995).

[3] M. Maldovan, Sound and heat revolutions in phononics, Nature **503**, 209 (2013).

[4] Z. Liu, X. Zhang, Y. Mao, Y. Y. Zhu, Z. Yang, C. T. Chan, and P. Sheng, Locally resonant sonic materials, Science **289**, 1734 (2000).

[5] S. Benchabane, A. Khelif, J.-Y. Rauch, L. Robert, and V. Laude, Evidence for complete surface wave band gap in a piezoelectric phononic crystal, Phys. Rev. E **73**, 065601 (2006).

[6] S. Mohammadi, A. A. Eftekhar, W. D. Hunt, and A. Adibi, High-Q micromechanical resonators in a two-dimensional phononic crystal slab, Appl. Phys. Lett. **94**, 051906 (2009).

[7] P. H. Otsuka, K. Nanri, O. Matsuda, M. Tomoda, D. M. Profunser, I. A. Veres, S. Danworaphong, A. Khelif, S. Benchabane, V. Laude *et al.*, Broadband evolution of phononic-crystal-waveguide eigenstates in real- and k-spaces, Sci. Rep. **3**, 3351 (2013).

[8] N. Boechler, G. Theocharis, and C. Daraio, Bifurcation-based acoustic switching and rectification, Nat. Mater. **10**, 665 (2011).

[9] V. Laude, L. Robert, W. Daniau, A. Khelif, and S. Ballandras, Surface acoustic wave trapping in a periodic array of mechanical resonators, Appl. Phys. Lett. **89**, 083515 (2006).

[10] S. Mohammadi and A. Adibi, On chip complex signal processing devices using coupled phononic crystal slab resonators and waveguides, AIP Adv. **1**, 041903 (2011).

[11] Y. Tsaturyan, A. Barg, E. S. Polzik, and A. Schliesser, Ultracoherent nanomechanical resonators via soft clamping and dissipation dilution, Nat. Nanotechnol. **12**, 776 (2017).

[12] S. H. Mousavi, A. B. Khanikaev, and Z. Wang, Topologically protected elastic waves in phononic metamaterials, Nat. Commun. **6**, 8682 (2015).

[13] C. He, X. Ni, H. Ge, X.-C. Sun, Yan-Bin Chen, M.-H. Lu, X.-P. Liu, and Y.-F. Chen, Acoustic topological insulator and robust one-way sound transport, Nat. Phys. **12**, 1124 (2016).

[14] C. Brendel, V. Peano, O. Painter, and F. Marquardt, Snowflake phononic topological insulator at the nanoscale, Phys. Rev. B **97**, 020102 (2018).

[15] N. Zen, T. A. Puurtinen, T. J. Isotalo, S. Chaudhuri, and I. J. Maasilta, Engineering thermal conductance using a two-dimensional phononic crystal, Nat. Commun. **5**, 3435 (2014).

[16] J. Maire, R. Anufriev, R. Yanagisawa, A. Ramiere, S. Volz, and M. Nomura, Heat conduction tuning by wave nature of phonons, Sci. Adv. **3**, e1700027 (2017).

[17] T. Kodama, M. Ohnishi, W. Park, T. Shiga, J. Park, T. Shimada, H. Shinohara, J. Shiomi, and K. E. Goodson, Modulation of thermal and thermoelectric transport in individual carbon nanotubes by fullerene encapsulation, Nat. Mater. **16**, 892 (2017).

[18] S. Mohammadi, A. A. Eftekhar, A. Khelif, and A. Adibi, Simultaneous two-dimensional phononic and photonic band gaps in opto-mechanical crystal slabs, Opt. Exp. **18**, 9164 (2010).

[19] K. Fang, M. H. Matheny, X. Luan, and O. Painter, Optical transduction and routing of microwave phonons in cavity-optomechanical circuits, Nat. Photon. **10**, 489 (2016).

[20] K. C. Balram, M. I. Davanco, J. D. Song, and K. Srinivasan, Coherent coupling between radiofrequency, optical and acoustic waves in piezo-optomechanical circuits, Nat. Photon. **10**, 346 (2016).

[21] M. Caleap and B. W. Drinkwater, Acoustically trapped colloidal crystals that are reconfigurable in real time, Proc. Natl. Acad. Sci. USA **111**, 6226 (2013).

[22] Y.-F. Wang, T.-T. Wang, Y.-S. Wang, and V. Laude, Reconfigurable Phononic-crystal Circuits Formed by Coupled Acoustoelastic Resonators, Phys. Rev. Appl. **8**, 014006 (2017).

[23] F. Casadei, T. Delpero, A. Bergamini, P. Ermanni, and M. Ruzzene, Piezoelectric resonator arrays for tunable acoustic waveguides and metamaterials, J. Appl. Phys. **112**, 064902 (2012).

[24] D. Hatanaka, I. Mahboob, K. Onomitsu, and H. Yamaguchi, Phonon waveguides for electromechanical circuits, Nat. Nanotechnol. **9**, 520 (2014).

[25] D. Hatanaka, A. Dodel, I. Mahboob, K. Onomitsu, and H. Yamaguchi, Phonon propagation dynamics in band-engineered one-dimensional phononic crystal waveguides, New J. Phys. **17**, 113032 (2015).

[26] J. Cha and C. Daraio, Electrical tuning of elastic wave propagation in nanomechanical lattices at MHz frequencies, Nat. Nanotechnol. **13**, 1016 (2018).

[27] D. Hatanaka, I. Mahboob, K. Onomitsu, and H. Yamaguchi, Mechanical random access memory in a phonon circuit, Appl. Phys. Exp. **7**, 125201 (2014).

[28] D. Hatanaka, T. Darras, I. Mahboob, K. Onomitsu, and H. Yamaguchi, Broadband reconfigurable logic gates in phonon waveguides, Sci. Rep. **7**, 12745 (2017).

[29] C. Chen, S. Rosenblatt, K. I. Bolotin, W. Kalb, P. Kim, I. Kymissis, H. L. Stormer, T. F. Heinz, and J. Hone, Performance of monolayer graphene nanomechanical resonators with electrical readout, Nat. Nanotechnol. **4**, 861 (2009).

[30] P. Weber, J. Güttinger, I. Tsioutsios, D. E. Chang, and A. Bachtold, Coupling graphene mechanical resonators to superconducting microwave cavities, Nano Lett. **14**, 2854 (2014).

[31] P. Weber, J. Güttinger, A. Noury, J. Vergara-Cruz, and A. Bachtold, Force sensitivity of multilayer graphene optomechanical devices, Nat. Commun. **7**, 12496 (2016).

[32] J. P. Mathew, R. N. Patel, A. Borah, R. Vijay, and M. M. Deshmukh, Dynamical strong coupling and parametric amplification of mechanical modes of graphene drums, Nat. Nanotechnol. **11**, 747 (2016).

[33] R. D. Alba, F. Massel, I. R. Storch, T. S. Abhilash, A. Hui, P. L. McEuen, H. G. Craighead, and J. M. Parpia, Tunable phonon-cavity coupling in graphene membranes, Nat. Nanotechnol. **11**, 741 (2016).

[34] N. Morell, A. Reserbat-Plantey, I. Tsioutsios, K. G. Schädler, F. Dubin, F. H. L. Koppens, and A. Bachtold, High quality factor mechanical resonators based on WSe_2 monolayers, Nano Lett. **16**, 5102 (2016).

[35] C. Lee, X. Wei, J. W. Kysar, and J. Hone, Measurement of the elastic properties and intrinsic strength of monolayer graphene, Science **321**, 385 (2008).

[36] A. Eichler, M. del Álamo Ruiz, J. A. Plaza, and A. Bachtold, Strong Coupling between Mechanical Modes in a Nanotube Resonator, Phys. Rev. Lett. **109**, 025503 (2012).

[37] O. L. Blakslee, D. G. Proctor, E. J. Seldin, G. B. Spence, and T. Weng, Elastic constants of compression-annealed pyrolytic graphite, J. Appl. Phys. **41**, 3373 (1970).

[38] M. Takamura, H. Okamoto, K. Furukawa, H. Yamaguchi, and H. Hibino, Energy dissipation in edged and edgeless graphene mechanical resonators, J. Appl. Phys. **116**, 064304 (2014).

[39] See the Supplemental Material at http://link.aps.org/supplemental/10.1103/PhysRevApplied.11.024024. Section 1 shows simulation results of comparison between unit structures with and without SiO_2 supports. Section 2 shows simulation results of comparison between electromechanical and pure mechanical approaches in FEM simulations.

[40] A. Reserbat-Plantey, K. G. Schädler, L. Gaudreau, G. Navickaite, J. Güttinger, D. Chang, C. Toninelli, A. Bachtold, and F. H. L. Koppens, Electromechanical control of nitrogen-vacancy defect emission using graphene NEMS, Nat. Commun. **7**, 10218 (2016).

[41] A. Castellanos-Gomez, M. Buscema, R. Molenaar, V. Singh, L. Janssen, H. S. J. van der Zant, and G. A. Steele, Deterministic transfer of two-dimensional materials by all-dry viscoelastic stamping, 2D Mater. **1**, 011002 (2014).

[42] K. Kang, K.-H. Lee, Y. Han, H. Gao, S. Xie, D. A. Muller, and J. Park, Layer-by-layer assembly of two-dimensional materials into wafer-scale heterostructures, Nature **550**, 229 (2017).

[43] M. Kurosu, D. Hatanaka, K. Onomitsu, and H. Yamaguchi, On-chip temporal focusing of elastic waves in a phononic crystal waveguide, Nat. Commun. **9**, 1331 (2018).